HAL
open science

Permeability of a Single Fracture; Validity of the Reynolds Equation

V. Mourzenko, Jean-François Thovert, P. Adler

To cite this version:

V. Mourzenko, Jean-François Thovert, P. Adler. Permeability of a Single Fracture; Validity of the Reynolds Equation. Journal de Physique II, 1995, 5 (3), pp.465-482. 10.1051/jp2:1995133 . jpa-00248173

HAL Id: jpa-00248173

https://hal.science/jpa-00248173v1

Submitted on 4 Feb 2008

HAL is a multi-disciplinary open access archive for the deposit and dissemination of scientific research documents, whether they are published or not. The documents may come from teaching and research institutions in France or abroad, or from public or private research centers.

L'archive ouverte pluridisciplinaire **HAL**, est destinée au dépôt et à la diffusion de documents scientifiques de niveau recherche, publiés ou non, émanant des établissements d'enseignement et de recherche français ou étrangers, des laboratoires publics ou privés.

J. Phys. II France **5** (1995) 465–482 MARCH **1995**, PAGE 465

Classification
Physics Abstracts
91.60B — 47.60 — 02.70

Permeability of a Single Fracture; Validity of the Reynolds Equation

V.V. Mourzenko(*), J.-F. Thovert, and P.M. Adler

LPTM/CNRS, Asterama 2, Avenue du Téléport, 86360 Chasseneuil du Poitou, France

(Received 17 October 1994, received in final form 1 December 1994, accepted 7 December 1994)

Abstract. — Single fractures are generated by statistical methods and described by a probability density of the profile heights and a spatial covariance function which is either Gaussian or self-affine. The results of numerical simulations based on both 2D Reynolds and 3D Stokes equations are presented. Total fluxes predicted by these equations for the same fractures are given and discussed. The difference between predictions of both models is analysed for the range of correlation lengths and apertures of real fractures, and it is found that the total fluxes for the same fractures may differ more than two times. When the local distance between the surfaces is used, the Reynolds equation provides much better results.

Introduction

Fluid flow through systems of interconnected fractures is often the main mechanism of fluid and solute transport in low-permeable rocks and is a subject of ongoing interest in petroleum engineering and hydrogeology. Real fractures are characterized by very heterogeneous structures of open space and it is important to correctly describe their hydraulic properties.

Numerical simulations of fluid flow in a single fracture are usually based on lubrication theory, and use the Reynolds equation for calculating the pressure distribution with a "cubic law" for the flux [1–3]

$$\nabla \cdot \left(\frac{b^3(x,y)}{12\mu} \nabla p \right) = 0 \tag{1}$$

$$Q_x = -L_y \frac{b^3}{12\mu} \frac{\partial p}{\partial x} \tag{2}$$

where b is the fracture aperture, p the fluid pressure, μ the viscosity and L_y the width of the fracture.

(*) *Permanent address:* Institute for Problems in Mechanics, Russian Academy of Sciences, 101, prosp Vernadskogo, Moscow, 117526, Russia.

© Les Editions de Physique 1995

The Reynolds equation can be derived from the Navier-Stokes equations for low velocity and a slowly varying aperture. It is difficult to estimate analytically the validity of the lubrication approximation and only a few quantitative comparisons are available. Using the results of [4,5], Zimmerman *et al.* [3] have found that the predictions of lubrication theory and of Stokes equations for the mean flux will not differ by more than 10% if the wavelength of the aperture oscillations exceeds $5\sigma_h$, where σ_h is the standard deviation of the profile height distribution. Another approach was used by Brown [2], with numerical solutions of Reynolds equation; the local ratio r of the velocity gradients parallel and perpendicular to the plane of the fracture was estimated; r should be small for the lubrication theory to be valid; r was found to be smaller than 0.1 if the wavelength of the aperture oscillations is larger than 50 σ_h; hence, the possible applications of Reynolds equation to natural fractures would seem to be severely restricted.

The major purpose of this work is to provide systematic results of numerical simulations based on the 2D Reynolds and 3D Stokes equations solved for the same fractures and to compare them. To the best of our knowledge, this has never been done. Fractures are described by a probability density of the profile height and by a correlation function. In this framework, two major classes of fractures are analysed, namely fractures with Gaussian or self-affine correlation functions; for sake of brevity, such fractures will be called Gaussian or self-affine. Two tentative definitions of the aperture used in the Reynolds equation (1) are given; in the first case, b is simply the vertical separation between the upper and lower surfaces; in the second case, the aperture b is replaced by an estimate of the actual distance between the two surfaces Permeabilities derived by the full Stokes equations and by the Reynolds equation based on b and b_d are systematically given as functions of the geometrical parameters.

It is emphasized that substantial differences between predictions of the exact Stokes equations and of the Reynolds equation based on b, are obtained for the range of correlation lengths and apertures of real fractures, for Gaussian and self-affine surfaces. However, when the aperture b_d is used in the Reynolds equation, the comparison is significantly improved.

This comparison is important for a precise determination of permeability. However, it may have also important consequences in other domains such as dispersion of solutes in fractures; the local distribution of the fluid velocity may substantially influence the determination of the dispersion tensor [6,7].

Generation of Fractures

The two surfaces of a fracture are described by the heights $z = h^{\pm}(x,y)$ above an arbitrary reference plane $z = 0$ (Fig 1). Usually, $h^{\pm}$ are random functions; they can be characterized by the two probability densities $\varphi(Z)$ and $\varphi(w)$ of the mean surface $Z = (h^+ + h^-)/2$ and of the distance $w = h^+ - h^-$ which are often assumed to be Gaussian

$$\varphi(F) = \frac{1}{\sqrt{2\pi}\sigma_F} \exp\left[-\frac{(F - \langle F\rangle)^2}{2\sigma_F^2}\right], \quad F = Z,\ w,\ h \tag{3}$$

where σ_F^2 denotes the variance $\langle (F - < F >)^2\rangle$. The brackets correspond to the statistical average.

The spatial correlations of the fields h^+ and h^- are described by the covariance functions $C_Z(r)$and $C_W(r)$, which are defined by

$$\begin{aligned} C_F(r) &= \langle \{F(x,y) - < F >\}\{F(x+\Delta x, y+\Delta y) - < F >\}\rangle \\ r &= (\Delta x^2 + \Delta y^2)^{1/2} \end{aligned} \tag{4a}$$

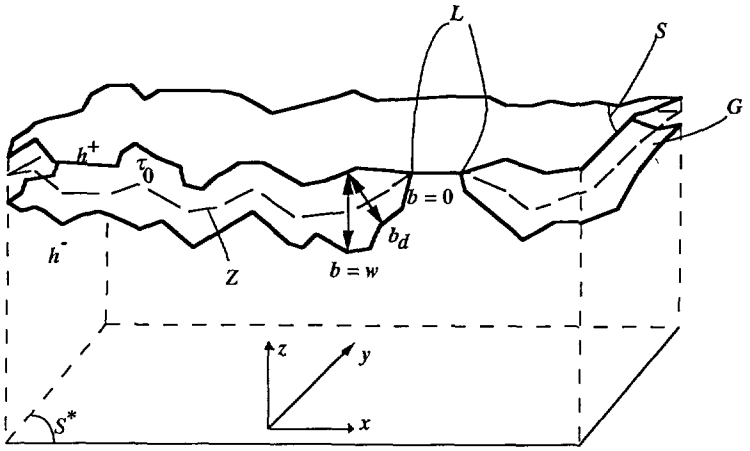

Fig. 1. — Conventions and notation for the fracture geometry. Only a unit cell is displayed.

For the so called Gaussian fractures, all the quantities h^+, h^-, Z and w were described by the quadratic covariance function

$$C_F(r) = \sigma_F^2 \exp\left(-\left(\frac{r}{l}\right)^2\right) \tag{4b}$$

with the same value l of the correlation length. Some attention will also be paid to structures with self-affine correlations $C_{h^\pm}(r)$ which are described at the end of this section.

In practice, spatially periodic fractures are built by juxtaposing identical elements of size $L \times L$, with $L \gg l$. The same approach was used for three-dimensional porous media [8].

The aperture b of a fracture is the difference between h^+ and h^- when it is non negative

$$b = \begin{cases} w, & w \geq 0 \\ 0, & w < 0 \end{cases} \tag{5a}$$

b may be described by its mean aperture $< b >$ and its variance σ_b^2, which are generally not equal to the mean separation $b_{\mathrm{m}} =< w >$ and to σ_w^2, respectively. When w is negative, the surfaces are considered to be in contact and one has $h^+ = h^- = Z$.

When the two surfaces of the fracture are very smooth, b is the natural aperture to choose. When this is not the case anymore, b has to be replaced by a better estimate of the local distance between the surfaces, which is inherent in the derivation of the Reynolds equation. Such an aperture can be defined in various ways. One of them consists of the determination of the diameter b_{d} of the largest sphere able to fit into the fracture at a given node. This method is derived from [9] for the topological characterization of porous media. Let $d_{\mathrm{s}}(x)$ denote the distance between the point x which is located in the void space, to the closest solid surface. $b_{\mathrm{d}}(x, y)$ may be formally defined by

$$b_{\mathrm{d}}(x, y) = 2 \max_{z \in [h^-, h^+]} d_{\mathrm{s}}(x, y, z) \tag{5b}$$

Instead of σ_Z, the standard deviation σ_h is used as a characteristic length because it may be directly estimated from measurements ($\sigma_h^2 = \sigma_Z^2 + \sigma_W^2/4$). The correlation between the two surfaces is characterized by the correlation parameter $\theta = 1 - \sigma_W^2/2\sigma_h^2$, which is 0 for uncorrelated surfaces and 1 for fully correlated surfaces All the possible situations can be

described by the three parameters b_m/σ_h, l/σ_h, and θ; this is equivalent to consider σ_h as the length unit.

To generate the random fields Z and w, the method of Fourier transforms is used (see [8] for details). Gaussian spatially correlated periodic fields were generated on a numerical grid (x_l, y_m) with $\Delta x = \Delta y = a$ and l, $m = 1, ..., N_c$ where N_c is the number of nodes in each direction. Some examples of vertical sections of generated fractures for different values of θ are presented in Figure 2. The influence of θ is clearly seen.

The useful range of parameters can be deduced from an analysis of the experimental data. If the quadratic covariance function (4) is used for h, the value l/σ_h may be found from

$$\frac{\mathrm{d}^2 C_h}{\mathrm{d}r^2}(r=0) = -\frac{2\sigma_h^2}{l^2} \tag{6}$$

This derivative is equal to $-m_2$, which is the second moment of the power spectrum of heights. Estimations of m_2 were presented in [10] for quartzite and granite; m_2 varied from 0.1 to 0.3 for fractures of different origins. Gentier [11] presented data for $\langle(\mathrm{d}h/\mathrm{d}x)^2\rangle$, which is a statistical estimation of $-C_h''(0)$, and found that it lies between 0.044 and 0.073. It is easy to find from (6) that l/σ_h varies between 2 and 7.

It is difficult to obtain direct estimates of b_m/σ_h, because b_m is a parameter of the model, while in practice $< b >$ is measured. But for a Gaussian distribution (3) of w, the value of b_m/σ_h may be estimated if $< b >$, σ_h or σ_b are given. Gentier [11] presented measured values of $< b >$, σ_h and σ_b. Using these data, b_m/σ_h was found to vary between 0.2 and 0.8. Brown

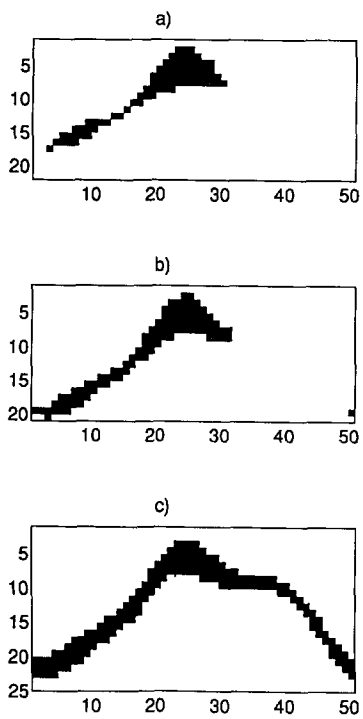

Fig. 2. — Simulated fracture profiles. $l/\sigma_h = 2$ and $b_\mathrm{m}/\sigma_h = 1$. Data are for: $\theta = 0.0$ (a), 0.5 (b) and 0.9 (c).

et al. [12] measured $< b >= 0.06 - 0.4$ mm, $\sigma_h = 0.23$ mm and $\sigma_b = 0.078$ mm; this implies $0 < b_m/\sigma_h < 2.6$.

To encompass all of these values, l/σ_h was varied from 1 to 7, b_m/σ_h from 0.5 to 5 and θ from 0 to 1. Values of b_m/σ_h less than 0.5 were not analysed because the fracture space is close to the percolation threshold, and the results of modelling require a refined finite-scale analysis.

Let us now address self-affine fractures since there exist many experimental observations where the self-affine character of rock surfaces is demonstrated [13]. Self-affine surfaces have features of a broad range of characteristic length scales and can be described by the covariance

$$C_h(r) \approx \sigma_h^2 \left(1 - \left(\frac{r}{\lambda}\right)^{2\zeta}\right) \tag{7}$$

where λ is a characteristic length and ζ is the roughness exponent [14]. For various materials, the exponent ζ was found to be 0.87 ± 0.07 [15].

The spectral density $G(k)$ is the Fourier transform of this covariance $C_h(r)$

$$G(k) = \frac{1}{4\pi^2} \int\int C_h(r) e^{ikr} d^2r \approx k^{-s} \tag{8}$$

where k is the wave number. The exponent s is given by

$$s = 2\zeta + 2 \tag{9}$$

s was found to vary between 3 and 4 for various rock surfaces [13]; this is in agreement with the previous estimation of [15].

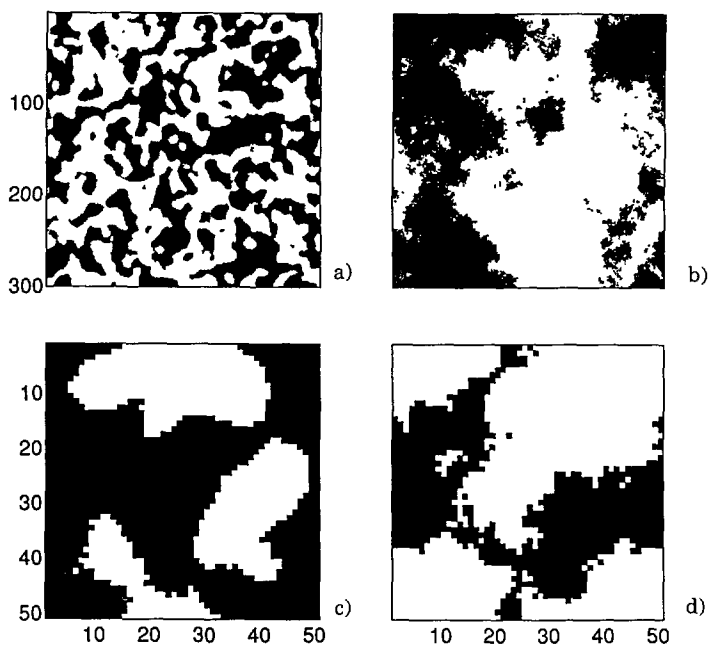

Fig. 3. — Distribution of contacts (white) between two generated surfaces with $b_m = 0$. Data are for $L/\sigma_h = 66$ (a-b), 11 (c-d), (a) and (c) correspond to Gaussian fractures with $l/\sigma_h = 2$; (b) and (d) correspond to self-affine fractures with $\zeta = 0\ 8$.

Since the method of Fourier transforms directly uses the Fourier transform of the covariance function (4a), the spectral density $G(k)$ can be used for the generation of fracture surfaces. Figure 3 shows distributions of contacts between two random surfaces which are generated by using the Gaussian covariance (4b) and the self-affine spectral density (8). The difference between the visual aspects of these two examples is striking.

It should be noticed that there are two cut-offs in the generation of self-affine fractures. The lower cut-off corresponds to the size of the elementary square a; the larger cut-off corresponds to the half-size of the unit cell itself. As for Gaussian fractures, spatially periodic conditions were used at the boundaries of the unit cell.

Stokes Equations

It is assumed in this paper that the velocities and characteristic dimensions are so small that inertial effects are negligible. Under these conditions which can be summarized by saying that the Reynolds number is vanishingly small, the Navier-Stokes equations can be replaced by the Stokes equations; this assumption is also valid when step-wise variations in aperture arise (cf. Fig. 2).

The analysis of Stokes flow is very similar to that made for three-dimensional porous media (cf. [8]). Consider an infinite fracture made of identical unit cells of size $L \times L$ in the (x, y)-plane. The low Reynolds number flow of an incompressible Newtonian fluid through a fracture is governed by the usual 3D Stokes equations

$$\nabla p = \mu \nabla^2 \mathbf{v}, \quad \nabla \cdot \mathbf{v} = 0 \tag{10}$$

where $\mathbf{v}$, p and μ are the velocity, pressure and viscosity of the fluid, respectively. In general, $\mathbf{v}$ satisfies the conditions

$$\mathbf{v} = 0, \quad \text{on the total surface } S \text{ of the fracture} \tag{11a}$$

and

$$\mathbf{v} \quad \text{is spatially periodic with period } L \text{ in the plane of the fracture} \tag{11b}$$

This system of equations and conditions applies locally at each point R of the interstitial fluid. In addition, it is assumed that the macroscopic pressure gradient $\overline{\nabla p}$ is specified,

$$\overline{\nabla p} = \frac{1}{\tau_0} \int_{\partial \tau_0} p \mathrm{d}s = \text{a prescribed constant vector} \tag{12}$$

where τ_0 is the volume of the fracture; τ_0 is bounded by the two solid surfaces S and the vertical boundary of the unit cell G, so that $\partial \tau_0 = S \cup G$ (see Fig. 1). The mean flow rate per unit fracture width $\overline{\mathbf{Q}_S}$ may be defined as

$$\overline{\mathbf{Q}_S} = \frac{1}{S^*} \int_{\tau_0} \mathbf{v} \cdot d^3\mathbf{r} \tag{13}$$

where S^* is the area of the (x, y)-projection of S. $\overline{\mathbf{Q}_S}$ is linearly related to the pressure gradient ∇p by the Stokes permeability tensor $\mathbf{B}_s$

$$\overline{\mathbf{Q}_S} = -\frac{1}{\mu}\mathbf{B}_s \cdot \overline{\nabla p} \tag{14}$$

$\mathbf{B}_s$ is a positive definite symmetric tensor which only depends on the geometry of the system; for isotropic fracture surfaces, the average tensor $\mathbf{B}_s$ may be simplified as $\mathbf{B}_s = B_s \cdot \mathbf{I}$, where $\mathbf{I}$ is the unit tensor. The value $b_S = (12B_s)^{1/3}$ is defined as the hydraulic aperture of a fracture as estimated from the Stokes equations.

Further details on some technical points such as the spatially periodic boundary conditions can be found in [8].

The numerical method which is used here is the so-called artificial compressibility method and is an improved version of that used in [16]. The problem is replaced by an unsteady compressible one which is assumed to converge towards the steady incompressible situation of interest. The equations were solved successively along each direction by using an alternating-direction-implicit scheme.

Convergence was reached when the flow rate was found to be the same within 1% across various sections of the medium. It sometimes took more than 104 iterations to obtain the solution. This number critically depends upon the geometry of the sample. The time step is limited by the occurrence of numerical instabilities and could not be increased during a given calculation to accelerate convergence.

A 50×50 mesh in the (x, y)-plane was used for most realizations. The number of nodes in the z-direction was varied from 25 to 40 and depended upon the distance $b_m \cdot \mathbf{B}_s$ varied of about 8% when N_c varied from 40 to 80. The step size a was usually equal to 0.2 σ_h and was increased to 0.45 σ_h for $b_m/\sigma_h = 10$. This discretisation is supposed to be small enough for a good representation of the vertical variations of the surface profiles. Since the correlation distance verifies $l/\sigma_h \geq 1$, the horizontal surface structures are also well represented (see Fig. 2).

It should be noted that the quadratic covariance function (4b) provides a random field which has no significant small scale features for lengths much smaller than l (Fig. 3a). The exponential decrease of correlations between heights at different points implies that the probability of appearance of large structures with a size $x \gg l$ is also negligible. This is not true for self-affine surfaces where structures of different length scales can appear with a comparable probability (Fig. 3b). The numerical method used here can be applied to flow in fractures with self-affine surfaces, but only if a limited range of characteristic length scales is taken into account, namely between the lower and upper cut-offs a and $L/2$ which were mentioned before.

Reynolds Equation

It is usually assumed that for very small Reynolds numbers and for slowly varying fractures, i.e. in the limit where b_m/σ_h and l/σ_h are large; the Navier-Stokes equations can be reduced locally to the two-dimensional Reynolds equation [3]

$$\nabla \cdot (b^3 \nabla p) = 0 \tag{15a}$$

Both definitions b and b_d (5a and b) can be used in this equation. When b_d is used, the resulting quantities are indexed by the subscript d.

Equation (15a) has to be supplemented by the no-flux boundary condition at the solid boundary L of the contact region (cf. also [17]). Let $\mathbf{n}$ be the normal in the xy-plane to the curve L; this condition reads as

$$\mathbf{n} \cdot \nabla p = 0 \quad \text{on } L \tag{15b}$$

The flow rate per unit fracture width $\mathbf{Q}$ is given by

$$\mathbf{Q} = -\frac{b^3}{12\mu} \nabla p \tag{16}$$

As previously, an infinite fracture made of identical unit cells of size $L \times L$ in the (x, y)-plane is considered. A complete analogy between the Reynolds equation and a two-dimensional diffusion problem exists (cf. [8]). It is supposed that $\mathbf{Q}$ is spatially periodic and $\overline{\nabla \mathbf{p}}$ is the same constant vector as in (12). In the same way, the mean flux $\overline{\mathbf{Q}_\mathrm{R}}$ is defined as

$$\overline{\mathbf{Q}_\mathrm{R}} = \frac{1}{S^*} \int_{S^*} \mathbf{Q} \mathrm{d}s \tag{17}$$

The Reynolds permeability tensor $\mathbf{B}_\mathrm{R}$ is readily defined by

$$\overline{\mathbf{Q}_\mathrm{R}} = -\frac{1}{\mu} \mathbf{B}_\mathrm{R} \cdot \overline{\nabla \mathbf{p}} \tag{18}$$

The hydraulic aperture is calculated from $b_\mathrm{R} = (12 B_\mathrm{R})^{1/3}$, where B_R is found after the averaging of $\mathbf{B}_\mathrm{R}$ over a large number of statistical realizations; again for statistically isotropic fractures, $\mathbf{B}_\mathrm{R} = B_\mathrm{R} \cdot \mathbf{I}$. The analogous quantities B_Rd and b_Rd will be often used in the following.

To solve the elliptic equation (15) together with the spatially periodic boundary conditions, the numerical "box integration method" is used (see [8, 18, 19]). The method was originally developed to solve usual diffusion equation with variable coefficients. The medium can be considered as the union of a set of elementary squares, over which b^3 is constant. The pressure field is defined at nodes, which are the corners of these elementary squares.

The elliptic equation (15a) is integrated over cells centered around each node. Truncated Taylor series are used for this integration. The discretized linear equation for the pressure field is obtained and is completed by overall boundary conditions. The set of equations for p was replaced by a time dependent one which is assumed to converge towards the steady solution. A time explicit scheme was used and in most cases an accurate solution is obtained in less than one thousand iterations.

Results and Discussion

The purpose of this study was to calculate solutions of the 2D Reynolds equation and of the 3D Stokes equations for the same fracture geometry and to compare them. The major portion of this section will address Gaussian fractures. Figure 4 shows generated aperture distribution and calculated flux fields for fractures with non-correlated surfaces ($\theta = 0$) for three of the four possibilities corresponding to the two values 1 and 3 of the ratios l/σ_h and $\mathrm{b_m}/\sigma_h$. The simulations were run on a $50 \times 50 \times 35$ mesh with a step size $a = 0.22\ \sigma_h$. The unit for the aperture fields b and b_d is chosen to be σ_h, in agreement with the previous conventions. The unit for the flow rate per unit fracture width Q is chosen to be $\sigma_h^3 \overline{\nabla p}/\mu$. Due to large differences between the maximal values of b and Q for various geometrical parameters of the generated fractures, different levels of shading are used; the choice of $b_\mathrm{m}^3 \cdot \overline{\nabla p}/\mu$. would certainly reduce these differences.

It is interesting to compare the first two rows. The overall shape of the aperture distributions is conserved, but with large quantitative differences.

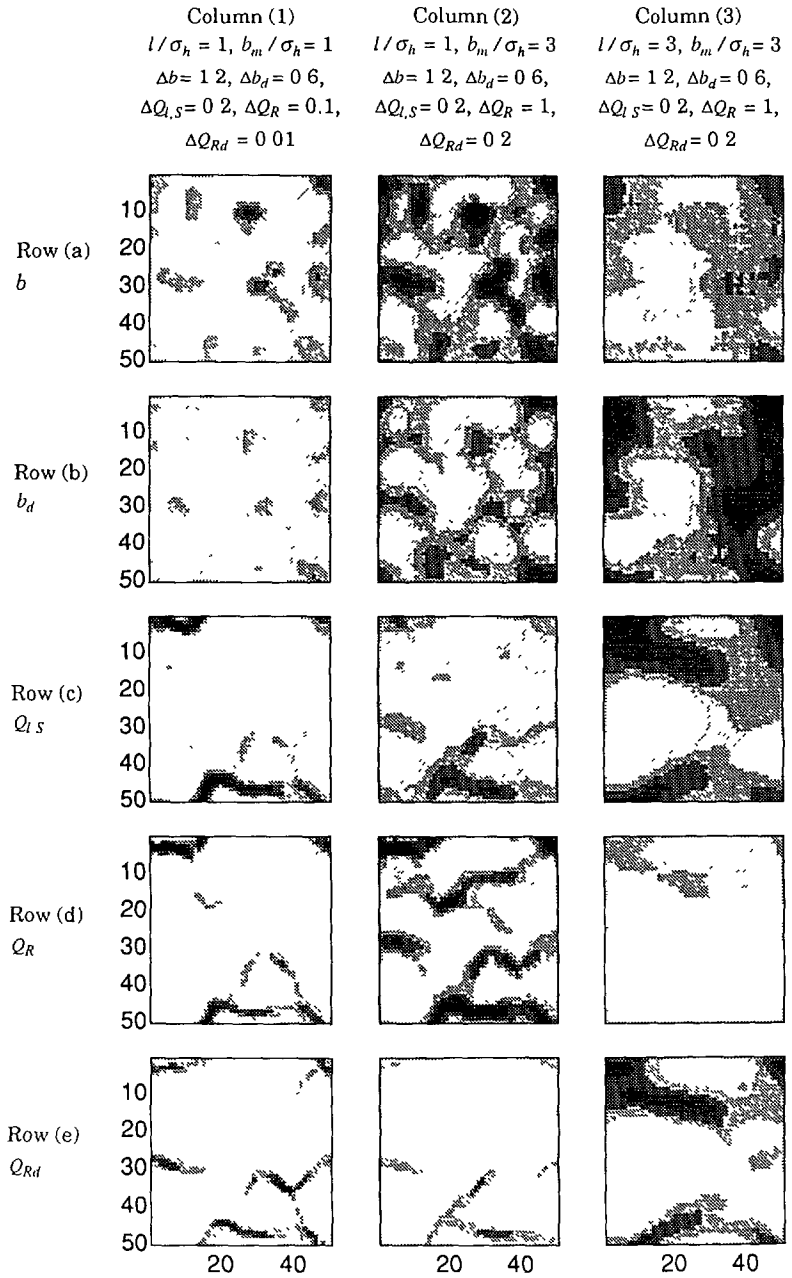

Fig. 4. — Simulated aperture and computed flux distributions over the fracture plane for non-correlated Gaussian fractures ($\theta = 0$). Six levels of shadings are distinguished from zero (white) to the largest value (dark). The shading steps for aperture are equal to Δb; for fluxes, they are equal to ΔQ. The three columns correspond to three combinations of the geometrical parameters l/σ_h and b_m/σ_h. The first two rows correspond to b and b_d with steps $\Delta b = 1.2$ and $\Delta b_d = 0.6$. The last three rows correspond to the three fluxes $Q_{l,S}$ (Stokes equations), Q_R (Reynolds equation with aperture b) and Q_{Rd} (Reynolds equation with aperture b_d)

It is easy to find that with decreasing b_m, the flow becomes more heterogeneous and fluid passes through several preferential flow paths (Figs. 4.c.1 and 2). This is the so-called channeling effect of fluid flow in fractures, which was observed experimentally [20] and described in numerical simulations [2,21]. Flow channeling appears for both Stokes and Reynolds flows (Figs. 4.1.c, d and e). For large values of the correlation length l/σ_h, flow channels become larger (Figs. 4.c.2 and 3) because the aperture b varies less with the distance than for low l (Figs. 4.a.2 and 3).

The general features of the flow distributions obtained by the Reynolds model with b and b_d are roughly the same, especially for small b_m/σ_h (Figs. 4 d.1 and e.1). This is due to the fact that the distribution of b_d approximately follows the distribution of b (Figs. 4a and b). The preferential flow paths are expected to be almost the same, because they are determined by the channels with the largest aperture.

In order to quantitatively compare the flow distributions between the Stokes and Reynolds models, the two cross-covariances were calculated

$$C_{fl} = \int_{S^*} (Q - \overline{Q}) \cdot (Q_{l,S} - \overline{Q_{l,S}}) \mathrm{d}s / \left[\int_{S^*} (Q - \overline{Q})^2 \mathrm{d}s \cdot \int_{S^*} (Q_{l,S} - \overline{Q_{l,S}})^2 \mathrm{d}s \right]^{1/2} \tag{19}$$

$$\overline{\mathbf{Q}_i} = \frac{1}{S^*} \int \mathbf{Q}_i \mathrm{d}s$$

The local flux $\mathbf{Q}_{l,S}$ in the Stokes approximation can be defined as

$$\mathbf{Q}_{l,S} = \int_{-h}^{h^+} \mathbf{v}(\mathbf{x}) \mathrm{d}z \tag{20}$$

The subscript l was added in order to avoid any confusion. The local flux $\mathbf{Q}$ in the Reynolds approximation is given by (16) where either b or b_d is used.

C_{fl} and C_{fld} are given in Table I for various values of l/σ_h and b_m/σ_h. These data correspond to a single fracture for each value of l/σ_h and θ. Note that for high b_m/σ_h, the flow distributions between the Stokes and Reynolds models are more different than they are for low b_m/σ_h. This trend can be observed for both Reynolds models and various values of l/σ_h and θ; this is not true anymore for small b_m/σ_h (see Tab I). This is surprising because the influence of surface roughness should decrease and because the flow distribution should approach the Poiseuille parabolic distribution, when b_m increases. For most realizations C_{fld} is found to be larger than $C_{fl} \cdot C_{fld}$ is about 0.9 when $b_m > l$, whereas it drops rapidly when the mean separation b_m becomes smaller than the correlation length l; the same statement holds for highly correlated surfaces ($\theta = 0.9$).

Figure 5 shows the same fields for highly-correlated surfaces ($\theta = 0.9$). It is obvious from the figures that a small value b_m of favours flow channeling in both models (Fig. 5.c-d, 1 and 2), but here flow is distributed over a larger number of flow paths than for $\theta = 0$. The difference in flow patterns obtained with Reynolds and Stokes equations increases when b_m increases for $\theta = 0.9$ as can be seen in Table I.

The overall permeabilities were analysed by means of the ratios

$$\frac{B_h}{B_{p_1}} = \left(\frac{b_h}{< b >} \right)^3 ; \quad \frac{B_h}{B_{p_2}} = \left(\frac{b_h}{b_m} \right)^3 , \quad h = S,\ R,\ R_d \tag{21}$$

where $B_{p_1} =< b >^3 /12$ and $B_{p_2} = b_m^3/12$ are the effective permeabilities of a plane channel of heights $< b >$ and b_m, respectively.

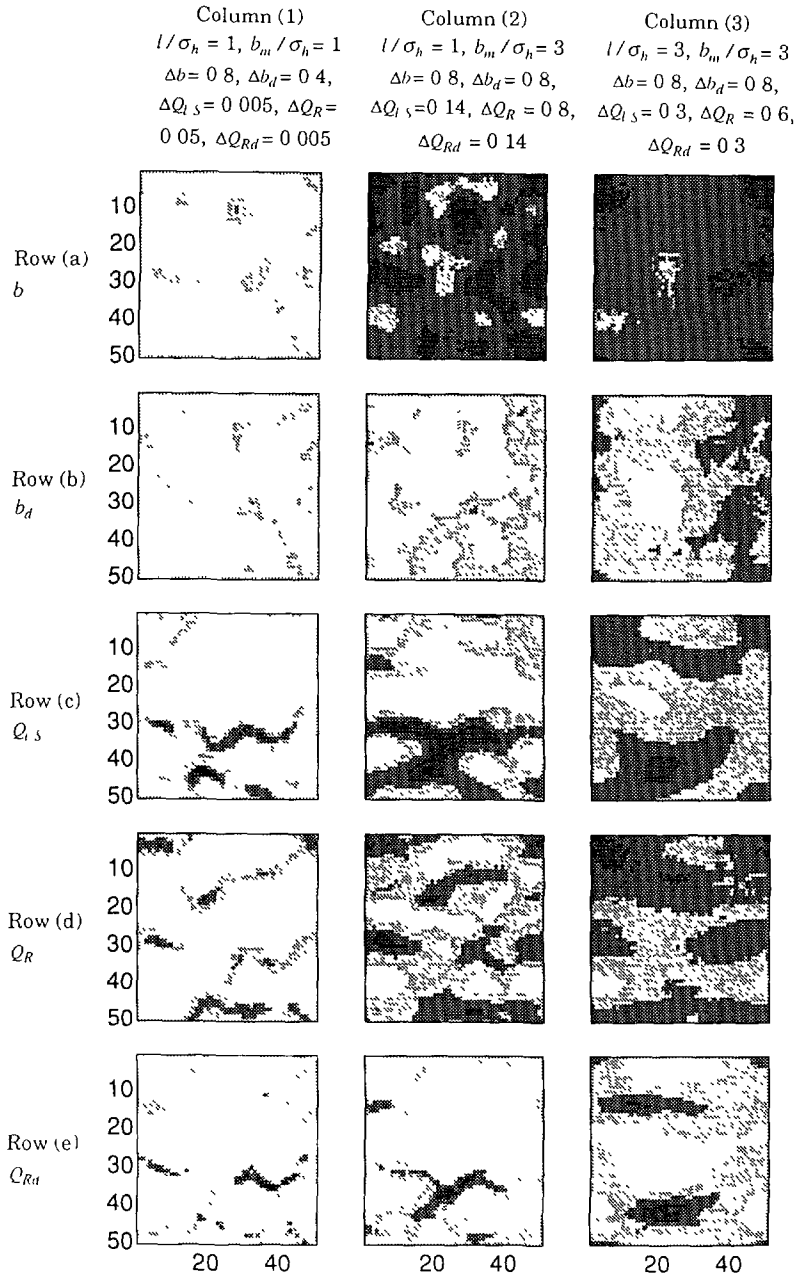

Fig. 5. — Simulated aperture and computed flux distributions over the fracture plane for correlated Gaussian fractures ($\theta = 0.9$). Six levels of shadings are distinguished from zero (white) to the largest value (dark) The shading steps for aperture are equal to Δb, for fluxes, they are equal to ΔQ. The three columns correspond to three combinations of the geometrical parameters l/σ_h and b_m/σ_h. The first two rows correspond to b and b_d. The three last rows correspond to the three fluxes $Q_{l,S}$ (Stokes equations), Q_R (Reynolds equation with aperture b) and Q_{Rd} (Reynolds equation with aperture b_d).

Table I. — *The cross-covariances C_{fl} and C_{fld} of local fluxes. Gaussian fractures.*

b_m/σ_h	C_{fl}	C_{fld}
$\theta = 0,\ l/\sigma_h = 1$		
10.0	0.57	0.84
6.0	0.68	0.91
3.0	0.81	0.92
2.5	0.82	0.91
2.0	0.83	0.92
1.5	0.84	0.89
1.0	0.83	0.73
0.5	0.79	0.26
$\theta = 0,\ l/\sigma_h = 3$		
10.0	0.90	0.93
6.0	0.91	0.94
3.0	0.95	0.95
2.5	0.96	0.95
2.0	0.96	0.50
1.5	0.96	0.83
1.0	0.84	0.34
0.5	-	-
$\theta = 0.9,\ l/\sigma_h = 1$		
10.0	0.21	0.84
6.0	0.13	0.86
3.0	0.43	0.88
2.5	0.43	0.88
2.0	0.47	0.87
1.5	0.52	0.87
1.0	0.56	0.78
0.5	0.57	0.24

For the same values of b_{m}, l and θ, several realizations of Z and w were used to obtain statistically representative results. All simulations were performed on a $50 \times 50 \times N_z$ mesh, where N_z was varied from 25 for $b_{\mathrm{m}}/\sigma_h \leq 2$ to 35 for $b_{\mathrm{m}}/\sigma_h = 5$. Comparison between simulations performed on this $50 \times 50 \times N_z$ mesh and simulations performed on a $80 \times 80 \times 50$ mesh, for $b_{\mathrm{m}}/\sigma_h = 1$, $l/\sigma_h = 1$, showed that b_{R}^3 and b_{S}^3 varied by only 8%. This is much smaller than the difference between Reynolds and Stokes models.

Each realization of pair of fracture surfaces has been combined for various values of b_{m}/σ_h. Eight values of b_{m}/σ_h ranging from 0.5 to 10 were used, while l/σ_h varied from 1 to 3. Ratios $B_h/B_{\mathrm{p_1}}$ averaged over 5 realizations of pairs of fracture surfaces are presented in Figure 6. One may conclude that if b is used as the local aperture in the Reynolds equation (15), the resulting mean flow rate is significantly larger than the one derived from the Stokes equation. The simulation with b_{d} yields a better approximation of B_{S}, at least for $b_{\mathrm{m}}/\sigma_h \geq 2$. Within the interval $2 \leq b_{\mathrm{m}}/\sigma_h \leq 10$, the trends of B_{S} and B_{Rd} are similar.

For $b_{\mathrm{m}}/\sigma_h < 2$, B_{Rd} undergoes large fluctuations with b_{m}/σ_h. This may be due to the fact that b_{m}/σ_h becomes comparable to the mesh size; hence, numerical results are not reliable anymore.

The calculated values of the ratios $B_{\mathrm{R}}/B_{\mathrm{p_1}}$ are in a good qualitative agreement with the

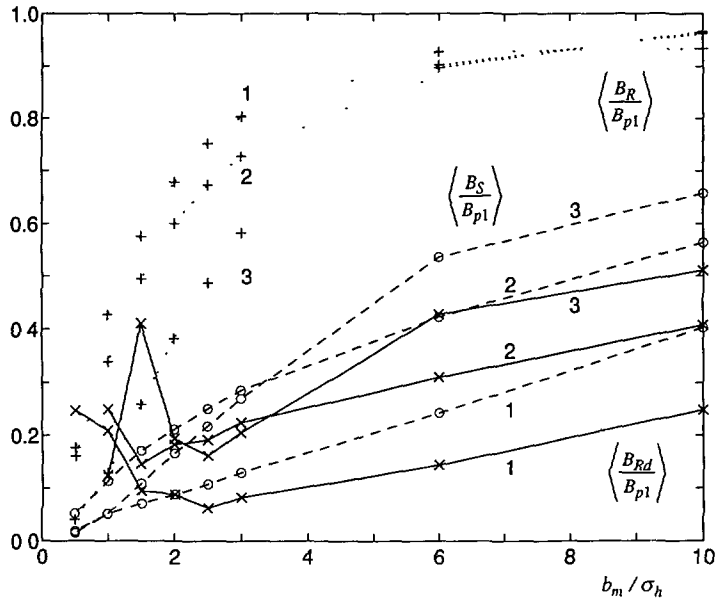

Fig. 6. — Dimensionless permeabilities $\langle B_{\mathrm{Rd}}/B_{p_1}\rangle$ (solid lines), $\langle B_{\mathrm{S}}/B_{p_1}\rangle$ (dashed lines), and $\langle B_{\mathrm{R}}/B_{p_1}\rangle$ (dotted lines) as functions of the mean separation b_{m}/σ_h for $\theta = 0$ and various l/σ_h (1, 2 and 3). Gaussian fractures.

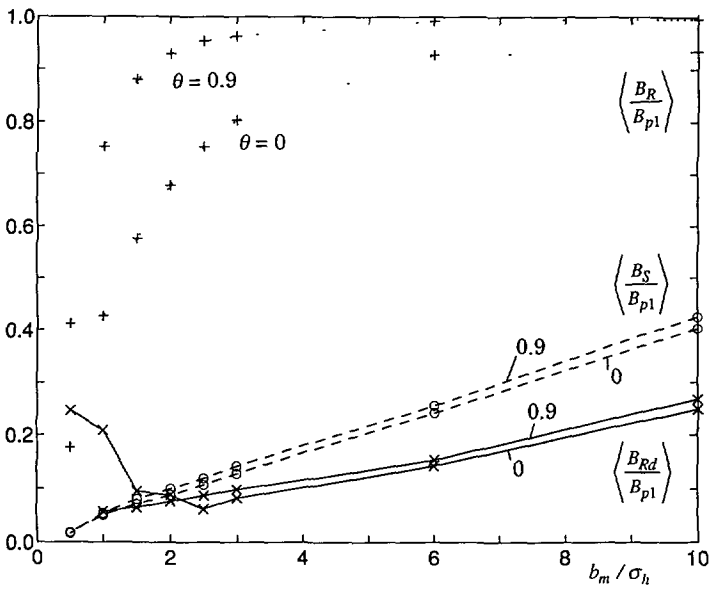

Fig 7. — Dimensionless permeabilities $\langle B_{\mathrm{Rd}}/B_{p_1}\rangle$ (solid lines), $\langle B_{\mathrm{S}}/B_{p_1}\rangle$ (dashed lines), and $\langle B_{\mathrm{R}}/B_{p_1}\rangle$ (dotted lines) as functions of the mean separation b_{m}/σ_h for $l/\sigma_h = 1$ and various θ (0 and 0 9) Gaussian fractures.

numerical results of Brown [2] who used the Reynolds equation (15) with the aperture defined by (5a). He found that B_R/B_{p_1} is unsensitive to the slope of the power spectrum of surface profiles, which defines the spatial correlation of surface roughness. The results of the present simulations also show that B_R/B_{p_1} does not depend upon l/σ_h for $b_m/\sigma_h \geq 6$ (Fig. 6). This is not true for B_S and B_{Rd}, which decrease with decreasing l/σ_h.

Figure 7 shows $\langle B_h/B_{p_1}\rangle$ for five realizations of fractures with correlated ($\theta = 0.9$) and uncorrelated ($\theta = 0$) surfaces. It is clear that θ only slightly influences B_S and B_{Rd} (for $b_m/\sigma_h \geq 2$), but largely influences B_R.

Hydraulic apertures are compared to the mean separation b_m of fracture surfaces in Figure 8. All the curves show the same trend; B_h/B_{p_2} is an increasing function of b_m/σ_h, for $b_m/\sigma_h \geq 1 \sim 2$; for $b_m/\sigma_h \leq 1 \sim 2$, the ratio B_h/B_{p_2} decreases with b_m/σ_h. It should be noted that the calculated values of the ratios B_R/B_{p_2} are also in agreement with the numerical results of [2]. As expected, for large fracture apertures, b_R, $< b >$ and b_m become equivalent, whereas b_{Rd} is significantly smaller. This is due to the fact that the distance b_d is very sensitive to all the asperities of the fracture surfaces. As a general rule, b_S lies between b_{Rd} and b_R.

Finally, the variations of $< B_R/B_S >$ and $< B_{Rd}/B_S >$ with the two parameters l/σ_h and b_m/σ_h are shown in Figures 9 and 10, and in Table II. Clearly, the best comparisons are observed for large values of b_m/σ_h and l/σ_h, i.e. for wide and smooth fractures. It was found that for $l/\sigma_h \leq 3$, $b_m/\sigma_h \leq 3$, the ratio $\langle B_R/B_S\rangle$ is always larger than 2 and depends slightly upon θ. This means that for the range of values l/σ_h and b_m/σ_h under consideration, the Reynolds equation with a locally distributed aperture (which is the difference between upper and lower surfaces) gives a total flow rate per unit fracture width more than 2 times larger than the Stokes equations. The difference is maximal for $l/\sigma_h = 1$, $b_m/\sigma_h = 0.5$, where the ratio reaches 9.2

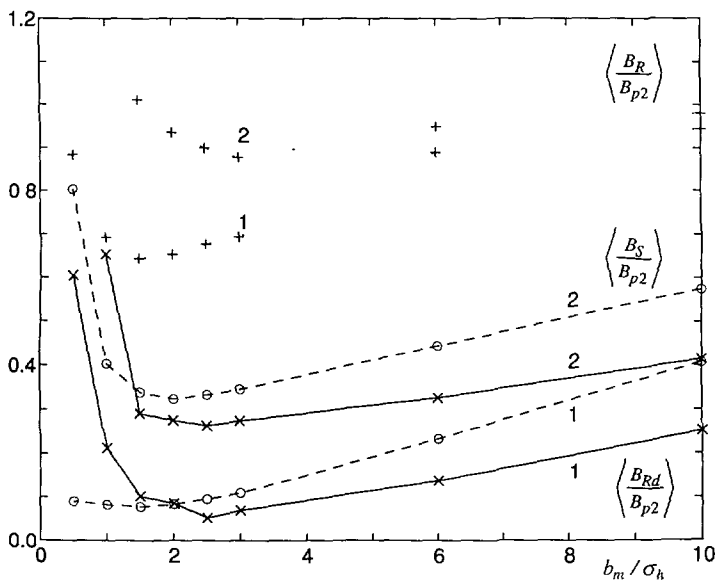

Fig. 8 — Dimensionless permeabilities $\langle B_{Rd}/B_{p_2}\rangle$ (solid lines), $\langle B_S/B_{p_2}\rangle$ (dashed lines), and $\langle B_R/B_{p_2}\rangle$ (dotted lines) as functions of the mean separation b_m/σ_h for $\theta = 0$ and various l/σ_h (1 and 2) Gaussian fractures.

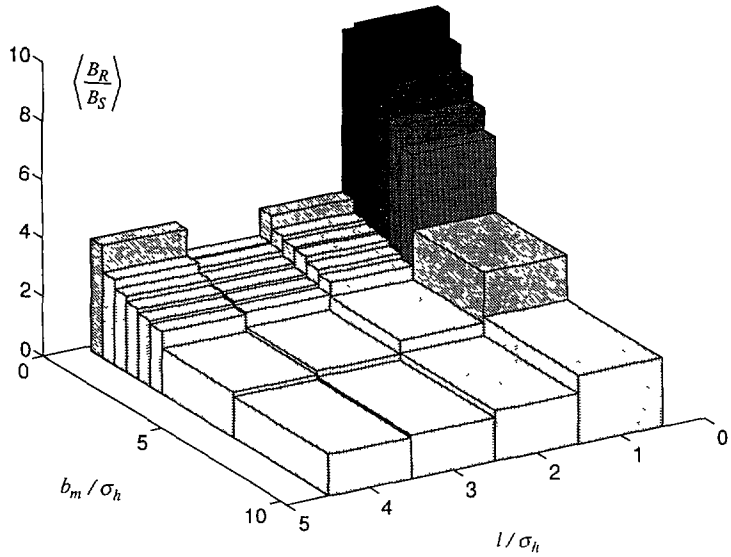

Fig. 9 — The ratio $\langle B_R/B_S \rangle$ as a function of $l/\sigma_h = 1$ and $b_m/\sigma_h = 1$ for Gaussian fractures with non-correlated surfaces ($\theta = 0$), b is used in the Reynolds equation. The block basis corresponds to $\langle B_R/B_S \rangle = 0$.

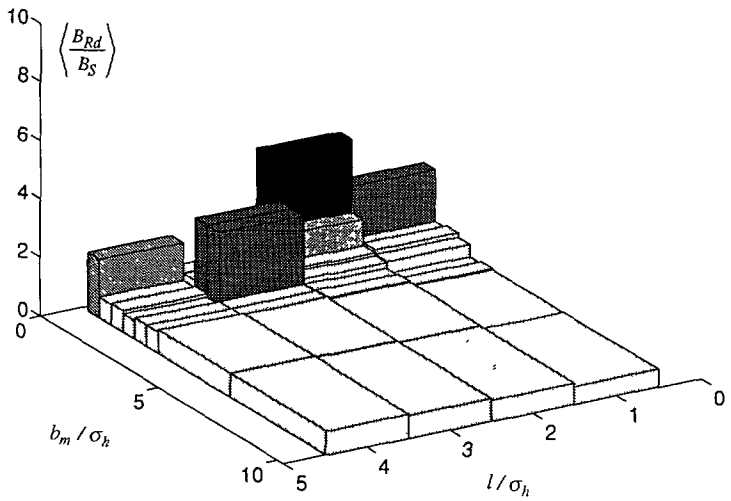

Fig. 10 — The ratio $\langle B_{Rd}/B_S \rangle$ as a function of l/σ_h and b_m/σ_h for Gaussian fractures with non-correlated surfaces; b_d is used in the Reynolds equation The block basis corresponds to $\langle B_{Rd}/B_S \rangle = 0$.

θ was not found to influence the ratio $< B_R/B_S >$ significantly, but simulations gave unexpected results. For highly correlated surfaces, the ratio B_R/B_S is greater than for uncorrelated surfaces ($\theta = 0$). This is surprising because for $\theta \approx 1$, the surfaces have almost the same form; the fracture aperture varies very slowly and one may expect that under these conditions, flow is close to a Poiseuille flow. Table II shows that the difference between the cases $\theta = 0.9$ and $\theta = 0$ is smaller than 60% for $l/\sigma_h = 1, b_m/\sigma_h \geq 1$ and that this difference decreases with l.

Table II. — *The ratio* $\langle B_R/B_S \rangle$ *as a function of* l/σ_h, b_m/σ_h *and* θ. *Gaussian fractures.*

b_m/σ_h	$l/\sigma_h = 1$		$l/\sigma_h = 3$	
	$\theta = 0$	$\theta = 0.9$	$\theta = 0$	$\theta = 0.9$
10.0	2.32	2.35	1.46	1.44
6.0	3.84	3.90	1.67	1.59
3.0	6.44	7.18	2.20	1.93
2.5	7.20	8.45	2.32	2.02
2.0	8.00	9.96	2.41	2.15
1.5	8.83	12.03	2.53	2.34
1.0	9.66	16.14	2.69	2.89
0.5	9.20	26.06	2.76	7.10

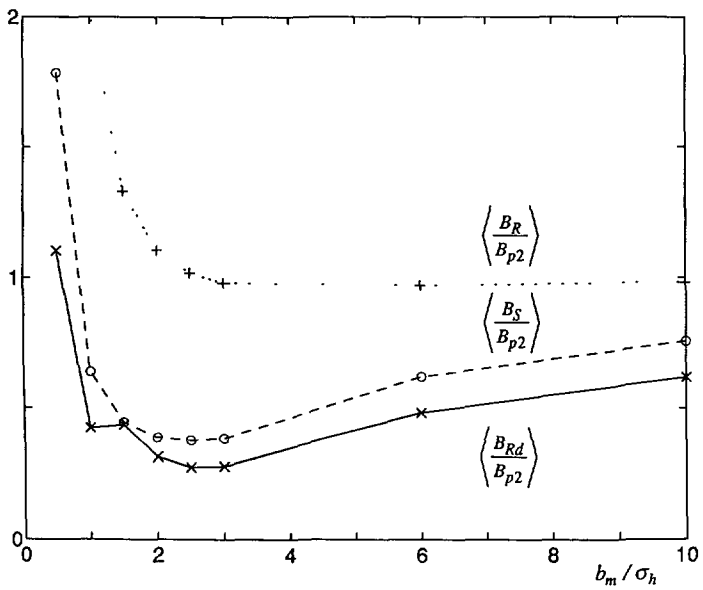

Fig. 11. — Dimensionless permeabilities $\langle B_{Rd}/B_{p_2} \rangle$ (solid lines), $\langle B_S/B_{p_2} \rangle$ (dashed lines), and $\langle B_R/B_{p_2} \rangle$ (dotted lines) as functions of the mean separation b_m/σ_h for self-affine fractures. Data are for· $\theta = 0$ and $\zeta = 0\ 8$.

The ratio $< B_{Rd}/B_S >$ is closer to 1 than $< B_R/B_S >$. The analysis of all the numerical data showed that b_{Rd} is a good approximation for b_S when b_m/σ_h is larger than 2 for uncorrelated surfaces ($\theta = 0$) and when b_m/σ_h is larger than 1 for highly correlated surfaces ($\theta = 0.9$).

It is found that if b_m/σ_h and l/σ_h become large enough ($b_m/\sigma_h > 7$, $l/\sigma_h > 5$), the ratio B_R/B_S tends toward 1 and the solution of the Reynolds equation with b defined in (5a) is a good approximation to the Stokes solution. If one of these parameters, b_m/σ_h or l/σ_h, is smaller than these limit values, the ratio B_R/B_S becomes larger than 1.

These results are relative to Gaussian fractures which are characterized by the correlation length l; it is seen from Figure 7 that the fracture permeability is only slightly influenced by the correlation parameter θ.

These computations were extended to self-affine surfaces since they are representative of real

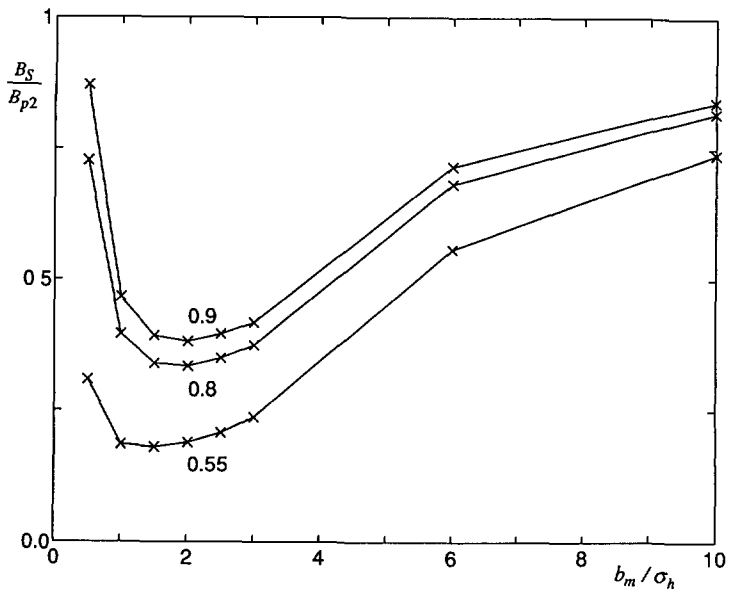

Fig. 12. — Dimensionless permeabilities B_S/B_{p_2} as functions of the mean separation b_m/σ_h for self-affine fractures with different ζ. Data are for: $\theta = 0$.

surfaces. Figure 11 shows mean permeabilities calculated for 5 realizations of uncorrelated self-affine surfaces with a roughness exponent $\zeta = 0.8$. It is useful to compare Figure 11 with Figure 8; the general shape of the curves is the same for Gaussian and self-affine surfaces. However, the permeability for self-affine surfaces is always larger than that of Gaussian surfaces; this may be related to the fact that the characteristic roughness length l is smaller for Gaussian surfaces than for self-affine surfaces where it is of the order of the total size of the sample because of the upper cut-off. The Reynolds equation does not provide a better approximation to permeability than before. However, the use of b_{Rd} instead of b yields a considerable improvement of the Reynolds approximation.

The influence of the roughness exponent ζ was analysed for the same realization of fracture surfaces (Fig. 12). It was found that B_S and B_{Rd} are decreasing functions of ζ, while B_R is insensitive to it; this finding is in good agreement with the numerical results of [2].

Conclusions

Fluid flow within fractures with randomly generated surfaces with Gaussian correlations was numerically studied using Stokes and Reynolds equations. Taking the solution of the Stokes equation as the reference, it was found that the Reynolds equation based on the aperture b (5a) overestimates the permeability by a factor larger than 2 in the range, $l/\sigma_h < 3$ and $b_m/\sigma_h < 3$. The ratio B_R/B_S varies slowly with l in an intermediate range, but grows sharply as l/σ_h tends to 1. This behavior is unaffected by a correlation between the fracture surfaces. The use of the aperture b_d in the Reynolds equation provides a much better approximation to B_S, which underestimates it.

This analysis was extended to fractures with self-affine correlations; the conclusions are basically the same for the validity of the approximation of the permeability by the Reynolds

equation. However, the use of the aperture b_d provides a better improvement than in the previous case.

This paper may be concluded by noting that real fractures may be much more complex than the idealization presented here. Most real fractures are found to contain fracture filling materials, etc., intersections and other perturbations that cause the proposed model to be generally incomplete. Moreover, the stationarity of the random fields is questionable. However, all these additional difficulties are better addressed by a local analysis of the velocity field by means of the Stokes equations

Acknowledgments

This work was partially supported by a grant from Ecotech. Part of the computations were performed at CNUSC.

References

[1] Tsang Y.W., and Tsang C.F., *Wat. Res Res.* **25** (1989) 2076.

[2] Brown S R., *J. Geophys. Res.* **92** (1987) 1337.

[3] Zimmerman R.W., Kumar S. and Bodvarsson G.S., *Int J. Rock Mech Min. Sci. Geomech Abstr.* **28** (1991) 325.

[4] Hasegawa E., and Izuchi H, *Bull JSME* **26** (1983) 514.

[5] Pozrikidis C., *J. Fluid Mech.* **180** (1987) 495.

[6] Koplik J., Ippolito I. and Hulin J.P , *Phys Fluids* **A5** (1993) 1333.

[7] Ippolito I., Daccord G , Hinch E.J. and Hulin J.P., *J Contam Hydrol.* **16** (1994) 87.

[8] Adler P.M , Porous Media: Geometry and Transports (Butterworth/ Heinemann, Stoneham, MA, 1992).

[9] Thovert J.F., Salles J. and Adler P.M., *J. Microsc* **170** (1992) 65.

[10] Brown S.R and Scholz C.H., *J Geophys Res.* **91** (1986) 4939.

[11] Gentier S , Morphologie et comportement hydromécanique d'une fracture naturelle dans le granit sous contrainte normale, Thesis, Université d'Orléans, France (1986).

[12] Brown S R , Kranz R.L. and Bonner B P., *Geoph Res. Lett.* **13** (1986) 1430.

[13] Brown S.R. and Scholz C.H., *J Geophys. Res* **90** (1985) 12575.

[14] Hansen A., Hinrichsen E.L. and Roux S., *Phys. Rev Lett.* **66** (1991) 2476.

[15] Måløy K.J., Hansen A., Hinrichsen E L. and Roux S , *Phys. Rev Lett.* **68** (1993) 213.

[16] Lemaître R. and Adler P.M , *Trans. Porous Media* **5** (1990) 325.

[17] Zimmerman R.W., Chen D.W. and Cook N G.W., *J Hydrol* **139** (1992) 79.

[18] Henriette A., Jacquin C.G and Adler P.M., *Phys Chem. Hydrodyn.* **11** (1989) 63.

[19] Yao J., Modélisation numérique de la porosité et de la perméabilité des roches, appliquée à la compréhension des problèmes d'injectivité dans les formations argilo-gréseuses, Thesis, Université de Paris - VI (1995) in preparation.

[20] Abelin H., Birgersson L., Gidlund J. and Neretnieks I., *Wat. Res Res.* **27** (1991) 3107.

[21] Moreno L , Tsang Y.W., Tsang C.F., Gale F.V. and Neretnieks I., *Wat. Res. Res.* **34** (1988) 2033